Graphite-Diamond Relations in Mantle Rocks: Evidence from an Eclogitic Xenolith from the Udachnaya Kimberlite (Siberian Craton) Revision 2

Denis S. Mikhailenko[a,*], Andrey V. Korsakov[a], Pavel S. Zelenovskiy[b], Alexander V. Golovin[a]

[a] *V.S. Sobolev Institute of Geology and Mineralogy of the Siberian Branch of the RAS, 3, Ac. Koptyuga ave., Novosibirsk 630090, Russian Federation*
[b] *Institute of Natural Sciences, Ural Federal University, Ekaterinburg, Lenin Ave. 51, 620000, Russia*

Abstract

Relations of graphite and diamond have been studied in a garnet-kyanite-clinopyroxene+sulfide+coesite/quartz+diamond+graphite eclogite xenolith from the Udachnaya-East kimberlite pipe in the Yakutian diamond province. Euhedral crystals of diamond and graphite occur in the intra- and intergranular space. The equilibrium conditions of diamond formation reconstructed by geothermobarometry for the Grt-Cpx-Ky-Coe mineral assemblage are 1020±40 °C and 4.7 GPa. Raman imaging of graphite enclosed in diamond shows high ordering and a 9 cm^{-1} shift of the ∼1580 cm^{-1} band. This Raman shift of graphite, as well as a 5 cm^{-1} shift of the 1332 cm^{-1} band of diamond, indicate large residual stress in graphite and in diamond around the inclusion, respectively. According to FTIR spectroscopy, nitrogen in diamond is highly aggregated and exists mainly as the A centers, while no other phases occur near graphite inclusions. Therefore, diamond in the analyzed eclogite sample must be quite old: it likely had crystallized long (∼1 Byr) before it became entrained with kimberlite melt.

New data show that graphite can stay in the upper mantle for billions of

*Corresponding author
Email address: mikhailenkodenis@gmail.com (Denis S. Mikhailenko)

years without converting to diamond. Crystallization of various carbon polymorphs, both in laboratory and natural systems, remains poorly constrained. Graphite present in mantle and UHP rocks may be a metastable phase crystallized in the diamond stability field. This fact should be taken into consideration when deducing petrological constrains and distinguishing diamond and graphite subfacies in upper mantle.

Keywords: Diamond, Graphite, Metastable graphite, Pseudomorphs, UHPM

Introduction

Graphite and diamond were identified as two upper mantle subfacies proceeding from graphite-to-diamond phase change (Dobretsov et al., 1974). The crystallization conditions for various polymorph modifications of carbon can be inferred from data on diamond- and graphite-bearing mantle rocks. The genesis of these rocks has been a subject of discussions for decades (Bobrievich et al., 1959; Pokhilenko et al., 1982; Robinson, 1979; Hatton, 1978; Robinson et al., 1984; Smyth and Caporuscio, 1984; Field and Haggerty, 1990; Pearson et al., 1990; Deines et al., 1991; Pearson et al., 1994; Viljoen, 1995; Korsakov et al., 2010; Naemura et al., 2011). According to earlier models (Bobrievich et al., 1959; Hatton, 1978; Robinson, 1979; Pokhilenko et al., 1982), diamond- and graphite-bearing eclogitic xenoliths entrained with erupting kimberlite magma crystallized close to the graphite-diamond equilibrium reaction curve. Pearson et al. (1994) hypothesized metastable growth of graphite within the diamond stability field and obtained the respective P-T (pressure and temperature) values for some graphite-bearing xenoliths.

Experimental studies of diamond crystallization from C-O-H fluids and in non-metallic systems, provide evidence that only diamond crystallizes at high temperatures while metastable graphite crystallization occurs at lower temperatures (Fig. 1) (Pal'yanov et al., 1999; Akaishi and Yamaoka, 2000; Akaishi et al., 2000; Yamaoka et al., 2000; Sokol et al., 2001b; Pal'yanov et al., 2002; Yamaoka et al., 2002a; Davydov et al., 2004; Pal'yanov et al., 2006). Ac-

This is a preprint, the final version is subject to change, of the American Mineralogist (MSA)
Cite as Authors (Year) Title. American Mineralogist, in press.
(DOI will not work until issue is live.) DOI: http://dx.doi.org/10.2138/am-2016-5657

cording to the experiments, carbon polymorphs crystallize in several successive steps with increasing temperatures and pressures: nucleation and growth of metastable graphite→nucleation and growth of metastable graphite+growth of diamond→nucleation and growth of diamond (Sokol and Pal'yanov, 2004; Pal'yanov et al., 2005).

Indeed, some graphite in UHP metamorphic rocks can crystallize within the diamond stability field (Korsakov et al., 2010) and survive in the metastable state due to very short duration of high-pressure metamorphism. On the other hand, diamond in mantle xenoliths crystallized in Archean-Proterozoic time (Jacob and Foley, 1999; Pearson et al., 1999), long before kimberlite intrusion, and all graphite in such xenoliths would have converted to diamond since then.

Graphite in mantle xenoliths is commonly found as isolated crystals among HP rock-forming minerals or as inclusions in them (Harris, 1972; Sobolev, 1974; Hatton and Gurney, 1979). Graphite inclusions in diamond are proto-, syn- or epigenetic (Harris and Gurney, 1979; Sobolev, 1974; Glinnemann et al., 2003; Nasdala et al., 2005; Bulanova et al., 1998; Meyer, 1987; Harris, 1992). Epigenetic graphite results from post-growth graphitization (Kuharenko, 1955) and occurs as discs or rosettes around fluid or mineral inclusions in diamond (Harris, 1972; Efimova et al., 1983). Protogenetic graphite, which serves as seeds for diamond crystallization, is euhedral and occurs mainly in the cores of diamond crystals (Bulanova et al., 1979; Bulanova, 1995; Glinnemann et al., 2003; Nasdala et al., 2003, 2005). Syngenetic inclusions are multi-phase and appear in cubic fibrous diamonds (Orlov, 1977; Zedgenizov et al., 2004) or in dark-gray octahedrons (Titkov et al., 2006; Logvinova et al., 2008), as well as in low mantle diamonds (Kaminsky et al., 2013).

The conditions and mechanisms responsible for the formation of different types of graphite inclusions in diamond long remained unclear until their features having implications for their genesis were revealed experimentally (Khokhryakov et al., 2009; Nechaev and Khokhryakov, 2013; Khokhryakov and Nechaev, 2015; Korsakov et al., 2015).

Protogenetic graphite inclusions have equant or round shapes (Khokhryakov

et al., 2009); their flakes are distributed unevenly over the diamond hosts, while round platelets are present in the host center. Diamond-hosted graphite grains show irregular or epitactic orientations and unevenly ordered structures.

Inclusions of syngenetic graphite were found in diamond synthesized upon seed crystals in non-metallic systems at different P, T, and h (time) (Khokhryakov et al., 2009). Graphite crystals were present all over diamond crystals and had euhedral hexagonal or irregular polygonal morphologies controlled by diamond growth layers. The diamonds were free from cracks and strain around the graphite inclusions (Khokhryakov et al., 2009; Khokhryakov and Nechaev, 2015). The Raman spectra of diamond-hosted graphite grains showed high ordering.

Epigenetic inclusions were obtained in experiments on ambient pressure high-temperature annealing of diamond (Nechaev and Khokhryakov, 2013). Diamond crystals enclosing epigenetic graphite were commonly cracked and compressed along {111}. Graphite grains occurred as equant hexagonal or round platelets, always coexisting with other mineral inclusions, localized along subgrain boundaries and cracks in the diamond-hosts. Their Raman spectra showed an ordered structure. The absence of epigenetic graphite inclusions in diamond from many deposits was attributed to low temperature (<900 °C) of kimberlite crystallization (Nechaev and Khokhryakov, 2013).

In this study we investigate relations between various carbon polymorphs in a diamond- and graphite-bearing eclogitic xenolith from the Udachnaya-East kimberlite in the Yakutian diamond province.

Geological setting

The Udachnaya pipe belongs to the Daldyn-Alakit field of the Yakutian kimberlite province in the Siberian craton (Fig. 2). The craton is a collage of 2.5 to 3.5 Ga terranes amalgamated by 1.8 - 2.1 Ga. Its Phanerozoic history included at least three major events of kimberlite magmatism in Upper Devonian to Lower Carboniferous (367 - 345 Ma), Triassic (245 - 215 Ma), and Upper

Jurassic (160 - 149 Ma) time (Davis et al., 1980; Brakhfogel, 1984; Kinny et al., 1997; Kostrovitsky et al., 2007).

The Udachnaya kimberlite results from the Middle Palaeozoic activity (367±5 Ma). The pipe consists of two bodies, the western and eastern ones, which differ in mineralogy, petrography, and in the alteration degree of xenoliths (Bobrievich et al., 1959; Kharkiv et al., 1991; Kostrovitsky et al., 2013; Kamenetsky et al., 2014). Mantle xenoliths from the Udachnaya-West kimberlite are commonly strongly serpentinised and more or less uniform, while those of Udachnaya-East are mainly fresh and highly diverse.

Analytical techniques

Mineral chemistry of main phases was determined at the Institute of Geology and Mineralogy (IGM, Novosibirsk, Russia), on a JEOL JXA-8100 electron microprobe operated at 20 kV acceleration voltage, 50 nA focused beam current and, 20-30 s counting time. A TESCAN MIRA 3 LMU JSM 6510LV equipped with an Oxford Instruments INCA energy detector, X-max 80 mm^2, was used for chemical mapping, at the operating conditions 20 kV, 1 nA, with an interval of 0.78 s for each spot (further analytical details can be found elsewhere in Lavrentev et al. (2015)).

Raman spectra in the range from 50 to 4000 cm^{-1} were recorded using a LabRam 800 HR(Horiba Jobin Yvon) spectrometer equipped with a 514.5 nm laser (power ×30 mW; beam diameter $\sim$ 1 μm).

Raman imaging of inclusions in diamond was performed using a WITec alpha300AR confocal Raman spectroscopy system at the Ural Center of Shared Use "Modern Nanotechnologies" (Ural Federal University, Ekaterinburg, Russia), at 488 nm laser wavelength, 70×70 μm mapping domain, resolution 140×140 points, and acquisition time 0.2 s at each point.

The isolated diamonds (core, mantle, and rim) were analyzed by FTIR spectroscopy, on a Bruker Vertex 70 FTIR spectrometer equipped with a HYPERION 2000 IR microscope, in the region 5000-6000 cm^{-1} (aperture 50×50 μm).

This is a preprint, the final version is subject to change, of the American Mineralogist (MSA)
Cite as Authors (Year) Title. American Mineralogist, in press.
(DOI will not work until issue is live.) DOI: http://dx.doi.org/10.2138/am-2016-5657

Petrography

The Uv-567 sample (5×7×5.8 cm) is a medium-grained eclogite with a massive structure and a granoblastic texture (Fig. 3), consisting of 60 vol.% round garnets, 30 vol.% residual anhedral clinopyroxene (CpxI), and 10 vol.% round coesite/quartz. Primary accessories in the sample are diamond, graphite, kyanite, rutile, pentlandite, pyrrhotite, and chalcopyrite; secondary phases are clinopyroxene (CpxII), K-feldspar, spinel, plagioclase, biotite, muscovite, chlorite, serpentine, quartz, and corundum.

Clinopyroxene appears in thin sections as two generations (Fig. 4C-D): 130×60 μm oval light-gray relict grains (CpxI) substituted by clinopyroxene-plagioclase symplectite (CpxII). The latter consists of fine milky white irregularly-shaped grains of clinopyroxene, plagioclase, and K-feldspar, varying in size from 10 to 50 μm away from residual CpxI.

Garnet exists as heavily cracked 0.8 to 4 mm reddish-orange round grains, with CpxII (diopside), plagioclase, amphibole, spinel, and sulfides along cracks; reaction rims around garnets are 30 to 50 μm thick.

All quartz in the sample is pseudomorphic after coesite, judging by typical palisade texture (Fig.5). The pseudomorphs are from 0.2 to 1.5 mm in matrix and $>$ 200 μm when occur as inclusions in garnet (Fig. 5); some are surrounded by chlorite and serpentine (Fig. 5) separated from quartz by a distinct boundary.

Rutile is the most abundant accessory in the sample, occurring as orange prismatic needles, 0.5 to 0.8 mm, most often at the garnet-symplectite boundary; it encloses numerous 10 to 15 μm lamelli of ilmenite.

Elongate prisms of light blue kyanite, 0.3-0.8 mm, occur only as inclusions in garnet (Fig. 6, 4A-B). Some kyanites are replaced by plagioclase-corundum and plagioclase-spinel symplectites, with pale to dark blue 150 μm long prisms of corundum set in a matrix of bluish-white plagioclase (12 to 50 μm). Euhedral spinel crystals, 15 to 50 μm, surround residual kyanites (Fig. 6B).

The sample contains two carbon polymorphs: diamond and graphite. Three macroscopic octahedral diamonds isolated mechanically from the central part

This is a preprint, the final version is subject to change, of the American Mineralogist (MSA)
Cite as Authors (Year) Title. American Mineralogist, in press.
(DOI will not work until issue is live.) DOI: http://dx.doi.org/10.2138/am-2016-5657

of the xenolith sample (Fig. 7) belong to variety I in the classification of Orlov (1977). Unevenly distributed graphite inclusions are present in all diamond crystals (mostly on grain periphery) but are especially abundant in one of them (Fig. 7A). They are surrounded by transparent penny-shaped cracks (Fig. 7) remaining within diamond grain. No other phases except the host diamond are observed in the cracks, as confirmed by FTIR and Raman spectroscopy data. Subhedral graphite flakes are mostly localized on {111} faces, together with negative oriented trigons.

The diamond faces have rough surfaces, apparently produced by growth, with negative trigons on {111} that form face-parallel chains, shield-shaped laminas, and grooves, as well as drop-shaped hillocks, mainly on face margins (Khokhryakov et al., 2002).

Euhedral graphite crystals, from 0.4 to 1 mm, occur as a residual phase in symplectite that substitutes for the primary pyroxene, as well as in garnet, where they are confined within grain boundaries (Fig. 8). Graphite in the sample shows no crystallographic preferred orientation. Most of graphite is enclosed in garnet, being surrounded by a fine aggregate of calcite, diopside, plagioclase, muscovite, biotite, and spinel. Graphite crystals also occur enclosed in diamonds (never in the core) or on their surfaces (Fig. 7C, F). Some round or polygonal graphite grains, from 15 to 250 μm in diameter, rise over diamond surfaces, being either isolated or less often forming clusters of aligned crystals. Graphite grains show different orientations relative to octahedral faces. Some have pinacoids (001) parallel to one of diamond faces (111).

Mineral chemistry

Garnet

Garnets span the pyrope-grossular-almandine range ($Prp_{37.2-43.3}Gross_{28.4-35.4}Alm_{21.9-25.8}$), with Mn components (Spess) within 0.4 mol.%. They are homogeneous within grains and have compositions typical of group B eclogites (Coleman et al., 1965). Contents of some elements vary

slightly over the sample. All garnets have high Na_2O (0.1 to 0.3 wt.%); CaO is from 11.8 to 13.5 wt.%; TiO_2 and MnO are within 0.1-0.3 and 0.1-0.2, respectively (Table 1). Calculated Fe^{3+} is from 0.28 to 0.6 wt.%; ratio Fe^{3+}/Fe^{tot} is from 3.2 to 5.5.

Clinopyroxene

Clinopyroxene is of two generations, which chemically belong to groups C and B (Taylor and Neal, 1989), respectively: omphacite ($Jd_{52.9-54.3}Di_{37.8-40.2}Hd_{5.1-5.6}CaTs_{0.2-1.6}$) and omphacite with a lower amount of jadeite ($Di_{48-54.4}Jd_{19.8-34.8}Hd_{4.8-8.5}En_{3.5-6.2}$). First-generation clinopyroxene is homogeneous and its major oxides vary from 0.1 to 0.2 wt.% K_2O, 7.2 to 7.8 wt.% Na_2O and 14 to 14.7 wt.% Al_2O_3. Later clinopyroxene is inhomogeneous and has its composition varying strongly within the sample. It has lower Na_2O (3.45 wt.%) and Al_2O_3 (10 wt.%) and lacks K_2O (Table 1).

Feldspars

Feldspar compositions vary markedly within the symplectite and depend on grain size. Plagioclase is albite according to its chemistry, with the compositions ($Ab_{93.2}An_{5.1}Or_{2.7}$) and ($Ab_{82}An_{16,2}Or_{1,8}$) of the largest and smallest grains, respectively. K-feldspar is sanidine ($Or_{85.6}Ab_{10.3}An_{2.7}$) coarse grains and ($Or_{89.3}Ab_{10.4}$) fine grains, which lack CaO, with K_2O from 10.5 to 14.3 wt.% (Table 1).

Raman spectroscopic results and IR

Typical Raman peaks of graphite from the Uv-567 sample are as in Fig. 9. The G-band of graphite inclusions in diamond, exposed on the (111) diamond faces, is very sharp at 1579 (±22 at 2 sigma) cm^{-1} (FWHM= 16-20 cm^{-1} in average) (Fig. 9A). There is a D1-band near 1350 cm^{-1} and a D2-band from 1616 to 1622 cm^{-1}. The second order Raman spectra of this type of graphite (Fig. 9B-E) show the main S1 peak at 2707-2716 cm^{-1} (FWHM= 71-80 cm^{-1} on average). The R2 ratio [D1/(G1+D1+D2)] ranges from 0.11 to 0.22. In the

second-order region, there is a sharp S1-band at 2713.7 cm^{-1} (FWHM = 76.5 cm^{-1}). There are also a sharp G-band at 1589.7 cm^{-1} (FWHM=21.4 cm^{-1}) and a lower D2-band at 1629.1 cm^{-1} (FWHM=21.4 cm^{-1}) (Fig. 10).

Diamond shows large residual strain around graphite inclusions as well as inside the latter (Fig. 11A). Residual pressure (compressive strain) in diamond is recorded in a 5.2 cm^{-1} shift of the 1331.8 cm^{-1} peak to 1337 cm^{-1} (Fig. 11A); the main diamond peak is shifted also in the central part of diamond crystals, to 1335 cm^{-1}. The residual compessive strain in diamond estimated by the method of Sharma et al. (1985) corresponds to a pressure of 2.2 GPa, and that in enclosed graphite, indicated by a 7 cm^{-1} shift of the G-band, is inferred to be $\sim$ 2 GPa.

Raman imaging revealed enclosed calcite next to the graphite inclusions in diamond (Fig. 12). Calcite shows peaks at 155 and 284 cm^{-1} and at 1088 cm^{-1}. Note that no graphite was observed around the calcite inclusion along the calcite-diamond boundary.

Nitrogen is the main impurity that controls many physical properties in diamond. The nitrogen content and speciation record the crystallization conditions of diamonds and their further thermal history (Boyd et al., 1987; Taylor et al., 1990; De Weerdt et al., 2003). Typical absorption bands in all analyzed crystals trace nitrogen defects A and B1, as well as a lamellar defect B2 marked by two absorption lines: a main line at 1370 cm^{-1} and a secondary line at 1430 cm^{-1}. Nitrogen varies in the range 900-1400 ppm, decreasing from core to rim, while its aggregation is from 38 % to 42 %. According to the obtained data, the diamonds belong to the widespread type IaA/B in the physical classification. FTIR spectroscopy of graphite enclosed in diamond (Fig. 13) has not revealed mineral or fluid phases within penny-shaped cracks associated with inclusions (points 4, 5, 6). At the same time, there are peaks of unknown origin at points 9, 10 and 11 in the 900-1000 cm^{-1} region.

Geothermobarometry

The assemblage garnet+clinopyroxene+phengite±kyanite±quartz/coesite is quite common in some Al-rich eclogites, and equilibria between these phases have successfully been used for independent estimation of pressure (P) and temperature (T) of HP and UHP rocks, which is otherwise impossible for most bi-mineral eclogites (Ravna and Paquin, 2003). In the kyanite-bearing eclogites, these reactions define an invariant point in both coesite and quartz stability fields, depending on which SiO_2 polymorph is stable. The geothermobarometric methods based on the net transfer reactions (1) in this system are less affected by later thermal re-equilibration than the conventional cation exchange thermometers, and make the estimation of Fe^{3+}/Fe^{tot} in omphacite and garnet less problematic (for temperature).

3 diopside + 2 kyanite = 1 grossular + 1 pyrope + 2 coesite/quartz (1)

The P-T conditions for eclogite sample Uv-567 with diamond and graphite were estimated using this geothermobarometer (Ravna and Paquin, 2003). The estimates were obtained using analyses of garnet cores and residual omphacite (CpxI). The pressure and the temperature were inferred to be 4.7±0.2 GPa and 1020±40 °C, respectively (Fig. 1). Interception of 40 mW/m^2 geothermal gradients (Pollack and Chapman, 1977) with temperatures estimated by geothermometer Ellis and Green (1979) provides very similar P-T conditions of 4.6 GPa and 1050 °C. The P-T conditions of pyroxene-plagioclase symplectite formation were estimated from the jadeite content in pyroxene (CpxII) (Holland, 1980, 1983; Aranovich and Perchuk, 1989). Coarse-grained symplectite crystallized at 2.3 GPa and 990 °C, while the fine-grained symplectite formed at 1.2 GPa and 600 °C (Fig. 1). Thus, the symplectite was apparently produced by metamorphism during xenolith transport, most likely with erupting kimberlite magma.

This is a preprint, the final version is subject to change, of the American Mineralogist (MSA)
Cite as Authors (Year) Title. American Mineralogist, in press.
(DOI will not work until issue is live.) DOI: http://dx.doi.org/10.2138/am-2016-5657

Discussion

The formation of graphite- and diamond-bearing eclogitic xenoliths is commonly considered in terms of crystallization of carbon polymorphs close to the diamond-graphite equilibrium reaction curve (Bobrievich et al., 1959; Hatton, 1978; Robinson, 1979; Pokhilenko et al., 1982). Crystallization of graphite is most often believed to be restricted to its stability field and either precede or postdate diamond formation (Bobrievich et al., 1959; Kuharenko, 1955; Hatton, 1978; Pokhilenko et al., 1982; Pearson et al., 1994; Nasdala et al., 2003, 2005).

However, there is experimental evidence (Litvin et al., 1997; Pal'yanov et al., 1999; Akaishi and Yamaoka, 2000; Akaishi et al., 2000; Yamaoka et al., 2000; Sokol et al., 2001b; Pal'yanov et al., 2002; Yamaoka et al., 2002a; Davydov et al., 2004; Pal'yanov et al., 2006) that metastable graphite can crystallize in the diamond stability field.

Crystallization of metastable graphite in natural samples was documented only in metamorphic rocks of the Kokchetav Massif where graphite survived due to brevity of the HP metamorphic event (Korsakov et al., 2010), but no direct proof for the possibility of metastable graphite growth in the mantle was found until recently.

Naemura et al. (2011) analyzed graphite-bearing peridotites of the Moldanubian zone in the Bohemian Massif and suggested two ways of graphite formation, either by precipitation from a relatively cold fluid or by graphitization of diamond. Graphite enclosed in garnet gave Raman peaks at 1350 cm^{-1} (D-1 band) and 1619 cm^{-1} (D-2 band) indicating low ordering (Naemura et al., 2011). On the other hand, Korsakov et al. (2015) showed that euhedral graphite crystals of a similar ordering degree could form from C-O-H fluids at 1300-1500 °C and a pressure of 2 GPa. Therefore, crystallization temperatures for fluid-derived graphite cannot be estimated from the graphite thermometer of Beyssac et al. (2002).

There is no literature on epigenetic graphite inclusions in diamond from the Udachnaya kimberlite. The Udachnaya kimberlite magma crystallized at tem-

This is a preprint, the final version is subject to change, of the American Mineralogist (MSA)
Cite as Authors (Year) Title. American Mineralogist, in press.
(DOI will not work until issue is live.) DOI: http://dx.doi.org/10.2138/am-2016-5657

peratures in the range 700-800 °C (Golovin et al., 2007) to 950-1100 °C (Sobolev et al., 1989) at the final stage. At such low temperature the graphitization of diamond crystal is very unlikely.

Experiments show that diamond graphitization in vacuum begins at a temperature no lower than 1150 °C and is very slow. As reported by Butenko et al. (2000), only small patches of carbon with a graphite structure appear on the diamond crystal surfaces for three hours at 1150 °C, which are detectable only in SEM images. In the analyzed sample, graphite grains are localized in diamond rims and partly rise over the surfaces, indicating that at least some graphite crystallized together with diamond.

The graphite inclusions are surrounded by transparent cracks remaining within the diamond grain. The cracks show no orientation along the {111} plane in diamond unlike epigenetic graphite inclusions produced by thermal and chemical interactions with kimberlite melt (Kuharenko, 1955; Harris and Vance, 1972; Nechaev and Khokhryakov, 2013; Khokhryakov and Nechaev, 2015). Diamond that encloses syngenetic and protogenetic graphite is commonly free from cracks and strain (Nechaev and Khokhryakov, 2013; Khokhryakov and Nechaev, 2015), but cracks appear around graphite and other mineral inclusions in natural diamond exposed to high temperatures in post-growth conditions (Harris and Vance, 1972). Disordered graphite is often present in penny-shaped cracks near graphite inclusions Nasdala et al. (2003). Graphitization in experiments reported by Harris and Vance (1972) began at 900 °C in cracks around inclusions (on dihedral angles), then proceeded to inclusion surfaces as the temperature rose further to 1000 °C and on to their margins. In our samples, penny-shaped cracks are free from other mineral phases, as follows from FTIR and Raman spectroscopy data. The calcite inclusion close to the graphite bears no graphitization signature at the calcite-diamond boundary. Judging by high nitrogen aggregation, the analyzed diamond remained exposed to a high temperature (thus staying in the mantle) for a long time (Evans and Qi, 1982).

Raman spectra of carbonaceous material are highly sensitive to its crystallinity. In the first-order region, a single Raman mode (G-band) is expected

at around 1580 cm^{-1} (Tuinstra and Koenig, 1970; Nemanich and Solin, 1979; Ferrari and Robertson, 2000). The D1-band and a shoulder at around 1620 cm^{-1} (D2) are typically observed in disordered carbonaceous material (Lespade et al., 1982; Wang et al., 1990; Wopenka and Pasteris, 1993; Pasteris and Wopenka, 2003). The Raman shift of the G-band towards higher frequencies records inclusions affected by compressive strain, as it happens in most diamond-hosted inclusions (Nasdala et al., 2003, 2005). The obvious inconsistency between remnant pressure 3.8 GPa (at P=4.7 GPa; T=293 °C; T_0=1020 °C) estimated for graphite inclusions using the model of Zhang (1998) and the respective estimates for graphite (2 GPa) and diamond (2.2 GPa) indicates partial stress release (Stepanov et al., 2011). This hypothesis agrees with the presence of transparent penny-shaped cracks around graphite inclusions in diamond crystals. Graphite in the sample we studied has a highly ordered structure (see above) and lacks D-1 and D-2 bands, which rules out poor ordering as a cause of G-band shifting (Beyssac et al., 2003).

According to the model of Zhang (1998), the shift of the main diamond peak to 1335 cm^{-1} may indicate diamond growth in several stages. This idea is consistent with rimward decrease in nitrogen ordering shown by FTIR spectroscopy. Nitrogen in the analyzed diamond crystals is quite highly aggregated, which is commonly attributed to high temperature during the post-growth history or to their prolonged exposure to the conditions of lithospheric mantle (Evans and Qi, 1982).

Experimental graphitization of synthetic diamonds in "dry" and "wet" systems at 2.0-2.5 GPa and different temperatures Korsakov et al. (2015) was uneven in different crystal faces. Graphitization in a "wet" system produced negative oriented trigons with sporadic euhedral flakes on {111} while coarse hexagonal graphites were localized on {100} and {110}. In the samples we studied, polygonal graphite grains mostly occur on {111}, together with negative oriented trigons and rounded edges and corners. Thus, the origin of graphite on diamond surfaces by graphitization via the coupled dissolution-precipitation process is unlikely, even in the presence of fluid, and cannot account for the

existence of graphite inclusions inside diamonds and in other minerals from the sample.

Finds of coarse graphite crystals in garnet (Fig. 8) likewise indicate that at least some graphite grains crystallized before garnet or simultaneously with it and other main phases at 4.7 GPa and 1020 °C (Fig. 1). The presence of graphite in interstitials, at garnet-symplectite boundaries, may testify for graphite crystallization together with a fine secondary phase aggregate at 1.2-2.3 GPa and 600-990 °C. The aggregate formed around graphite grains at a late stage, most likely during kimberlite intrusion rather than during C-O-H fluids percolation. Similar secondary products detected near diamond crystals free from graphite signatures indicate that graphite likely formed together with primary minerals of eclogite: garnet, pyroxene, coesite and kyanite. Note additionally that graphite grains are about ten times larger than those of secondary phases and thus must have formed simultaneously with other main minerals at higher pressures and temperatures. If graphite crystallization occurred together with the formation of spongy texture, its rate was several times as high as for low-pressure rock-forming minerals. Given that the ascent of kimberlite melt from a depth of 200 km takes 72 hours (Spera, 1984; Pearson et al., 1997; Meyen, 1985; Canil and Fedortchouk, 1999), the graphite crystallization rate must exceed 0.016 mm/hr (or 0.012 mm/hr at 100 hours of ascent). The presence of diamond in the eclogite sample may be due to percolation of C-O-H fluids (Taylor et al., 1998; Anand et al., 2004; Stepanov et al., 2007, 2008; Shatsky et al., 2008; Liu et al., 2009) and thus may be associated with metasomatism. Inasmuch as the host mineral fails to buffer all graphite (Fig. 8), the latter hardly can be expected to survive in metasomatism, judging by the results of experiments by Yamaoka et al. (2002b) where all graphite converted to diamond for 8-10 hours at 7.7 GPa and 1500 °C. Preservation of graphite in diamond was also possible if the zones with graphite eluded the effect of the C-O-H fluids, which only partly penetrated into the rock.

Thus, graphite inside garnet, clinopyroxene and diamond crystals and, possibly, also on their surfaces, crystallized in the diamond stability field rather

than being a product of partial graphitization of diamond. It remains unclear why different carbon polymorphs crystallize, both in natural and laboratory conditions. Diamond formation is most often predicted to occur at upper mantle pressures and temperatures and at moderate fO_2 (Sobolev, 1974; Haggerty, 1986, 1999; Meyer, 1987; Harris, 1992; Schrauder and Navon, 1994; Navon, 1999; Luth, 1999, 2001), while graphite crystallizes in more reduced settings (Sokol and Pal'yanov, 2004; Sokol et al., 2004). Graphite and diamond crystallization may be controlled by fO_2 (Sokol and Pal'yanov, 2008). Nevertheless, graphite is always the earliest phase to crystallize in the diamond stability field, among carbon polymorphs, in experimental diamond synthesis in non-metallic systems (Sokol and Pal'yanov, 2008). Unlike HP metamorphic rocks, where metastable graphite survives due to brevity of HP metamorphism, diamond with highly aggregated nitrogen from eclogitic xenoliths had formed about 1 Byr before the latter became entrained with kimberlite magma (Stepanov et al., 2007).

Experimental studies of diamond crystallization in non-metallic systems reveal that fO_2 play important role in diamond formation, in addition to pressure and temperature the (Fig. 1) (Pal'yanov et al., 1999; Akaishi and Yamaoka, 2000; Akaishi et al., 2000; Yamaoka et al., 2000; Sokol et al., 2001b; Pal'yanov et al., 2002; Yamaoka et al., 2002a; Davydov et al., 2004; Pal'yanov et al., 2006). Diamond crystallization occurs from C-O-H fluids at moderately oxidized conditions, while only graphite precipitated in reduced conditions even in the diamond stability field (Sokol et al., 2001b; Pal'yanov and Sokol, 2009). However, as it was recently demonstrated by Sverjensky and Huang (2015), diamond crystallization is possible without redox change. Graphite-diamond crystallization requires higher pH, which occurs naturally upon water-mantle interaction at certain conditions. This new model of reactions in the lower crust and upper mantle calls for revision of the global carbon cycle patterns. Unfortunately, the estimation of pH for natural samples remains almost impossible, and we cannot test this model for our sample. Furthermore, FTIR-spectroscopy of the diamond crystal did not reveal H_2O. The presence of calcite inclusions in diamond close to graphite may indicate that carbon polymorphs were derived

from carbonatite melt.

Stagno et al. (2015) discussed the role of oxygen fugacity in carbonate melts in eclogites during diamond and graphite crystallization in their own stability field and constrained the stability fields for carbonate melt, graphite and diamond, depending on the depth and oxygen fugacity. The calculated Fe^{3+}/Fe^{tot} ratios for the eclogitic garnets from sample the Uv-567 are in good agreement with the estimated values of fO_2 for eclogite assemblages obtained by Stagno et al. (2015) for diamond/graphite precipitats. In general, primary omphacitic clinopyroxene of the kyanite-bearing eclogites are completely replaced by clinopyroxene-plagioclase symplectites, which makes fO_2 estimation for these samples more complicated. In the presence of kyanite and SiO_2 polymorphs, cabonates may also change oxygen fugacity, as it was recently proposed by Frezzotti et al. (2014). We have not measured Fe^{3+} concentration in our eclogite sample yet, but expect to do it in the nearest future.

Implications

The reported finds of graphite inclusions in diamond from the eclogitic xenolith sample provide the first evidence of metastable graphite crystallization in the diamond stability field in the upper mantle, much below ($\pm$20 km) the graphite-diamond equilibrium. Proceeding from high nitrogen aggregation, the presumed old age of graphite-bearing diamond crystals indicates that graphite can stay in the upper mantle within the field of diamond stability for a long time. This fact has to be taken into account in petrological reconstructions and in identification of upper mantle facies.

Acknowledgement

We greatly appreciate the assistance of our colleagues from IGM (Novosibirsk): E.N. Nigmatulina for EMPA, I.N. Kupriyanov for FTIR spectroscopy of diamonds, A.L. Ragozin for preparing samples for analyses and E. N. Fedorova

for interpretation FTIR data. Thanks are extended to A. Shatskiy for interpretations of data during the manuscript preparation. The paper profited much from constructive criticism by G. Yaxley and an anonymous reviewer.

The study was supported by grant RSF №15-17-30012 from the Russian Science Foundation and was carried out using the equipment of the Ural Center of Shared Use "Modern Nanotechnologies" supported by the Ministry of Education and Science of the Russian Federation (unique identifier RFMEFI59414X0011).

Akaishi, M., Kumar, M. S., Kanda, H., and Yamaoka, S. (2000) Formation process of diamond from supercritical H_2O–CO_2 fluid under high pressure and high temperature conditions. Diamond and related materials, 9, 1945–1950.

Akaishi, M. and Yamaoka, S. (2000) Crystallization of diamond from C–O–H fluids under high-pressure and high-temperature conditions. Journal of Crystal Growth, 209, 999–1003.

Anand, M., Taylor, L. A., Misra, K. C., Carlson, W. D., and Sobolev, N. V. (2004) Nature of diamonds in Yakutian eclogites: views from eclogite tomography and mineral inclusions in diamonds. Lithos, 77, 333–348.

Aranovich, L. Y. and Perchuk, A. L. (1989) Experimental study of equilibrium clinopyroxene + quartz + albite in the system Na_2O-CaO-FeO-Al_2O_3-SiO_2 at 14-25 kbar and 900-1100^{o}C. Doklady Akademii Nauk SSSR, 307, 1453–1457.

Beyssac, O., Goffé, B., Chopin, C., and Rouzaud, J. N. (2002) Raman spectra of carbonaceous material in metasediments: a new geothermometer. Journal of metamorphic Geology, 20, 859–871.

Beyssac, O., Goffé, B., Petitet, J.-P., Froigneux, E., Moreau, M., and Rouzaud, J.-N. (2003) On the characterization of disordered and heterogeneous carbonaceous materials by Raman spectroscopy. Spectrochimica Acta Part A: Molecular and Biomolecular Spectroscopy, 59, 2267–2276.

462 Bobrievich, A. P., Smirnov, G. I., and Sobolev, V. S. (1959) Eclogite xenolith
463 with diamonds. Doklady Akademii Nauk, 126, 637–640.

464 Bose, K. and Ganguly, J. (1995) Quartz-coesite transition revisited: Reversed
465 experimental determination at 500-1200 ^{o}C and retrieved thermochemical
466 properties. American Mineralogist, 80, 231–238.

467 Boyd, S. R., Mattey, D. P., Pillinger, C. T., Milledge, H. J., Mendelssohn,
468 M., and Seal, M. (1987) Multiple growth events during diamond genesis: an
469 integrated study of carbon and nitrogen isotopes and nitrogen aggregation
470 state in coated stones. Earth and Planetary Science Letters, 86, 341–353.

471 Brakhfogel, F. F. (1984) Geological aspects of kimberlite magmatism in the
472 northeastern Siberian platform. Siberian Branch of Academy of Sciences of
473 USSSR, 128, 130–135.

474 Bulanova, G., Griffin, W., and Ryan, C. (1998) Nucleation environment of dia-
475 monds from Yakutian kimberlites. Mineralogical Magazine, 62, 409–419.

476 Bulanova, G. P. (1995) The formation of diamond. Journal of Geochemical
477 Exploration, 53, 1–23.

478 Bulanova, G. P., Varshavskiy, A. V., Leskova, N. V., and Nikishova, L. V. (1979)
479 On "central" inclusions in natural diamonds. Doklady Akademii Nauk SSSR,
480 244, 704–706.

481 Butenko, Y. V., Kuznetsov, V. L., Chuvilin, A. L., Kolomiichuk, V. N., Stankus,
482 S. V., Khairulin, R. A., and Segall, B. (2000) Kinetics of the graphitization of
483 dispersed diamonds at "low" temperatures. Journal of Applied Physics, 88,
484 4380–4388.

485 Canil, D. and Fedortchouk, Y. (1999) Garnet dissolution and the emplacement
486 of kimberlites. Earth and Planetary Science Letters, 167, 227–237.

487 Coleman, R. G., Lee, D. E., Beatty, L. B., and Brannock, W. W. (1965) Eclogites
488 and eclogites: their differences and similarities. Geological Society of America
489 Bulletin, 76, 483–508.

Davis, G. L., Sobolev, N. V., and Kharkiv, A. D. (1980) New data on the age of Yakutian kimberlites U-Pb zircon method. Doklady Akademii Nauk SSSR, 254, 175–179.

Davydov, V. A., Rakhmanina, A. V., Agafonov, V., Narymbetov, B., Boudou, J.-P., and Szwarc, H. (2004) Conversion of polycyclic aromatic hydrocarbons to graphite and diamond at high pressures. Carbon, 42, 261–269.

De Weerdt, F., Pal'yanov, Y. N., and Collins, A. T. (2003) Absorption spectra of hydrogen in ^{13}C diamond produced by high-pressure, high-temperature synthesis. Journal of Physics: Condensed Matter, 15, 3163.

Deines, P., Harris, J. W., Robinson, D. N., Gurney, J. J., and Shee, S. R. (1991) Carbon and oxygen isotope variations in diamond and graphite eclogites from Orapa, Botswana, and the nitrogen content of their diamonds. Geochimica et Cosmochimica Acta, 55, 515–524.

Dobretsov, N. L., Sobolev, V. S., Sobolev, N. V., and Khlestov, V. V. (1974) The facies of regional metamorphism at high pressure. Nedra, 328.

Efimova, Y. C., Sobolev, N. V., and Pospelova, L. N. (1983) Sulphide inclusions in diamonds and features of their paragenesis. Zapiski VMO, 3, 300–310.

Ellis, D. and Green, D. (1979) An experimental study of the effect of Ca upon garnet-clinopyroxene Fe-Mg exchange equilibria. Contributions to Mineralogy and Petrology, 71, 13–22.

Evans, T. and Qi, Z. (1982) The kinetics of the aggregation of nitrogen atoms in diamond. Proceedings of the Royal Society of London. A. Mathematical and Physical Sciences, 381, 159–178.

Ferrari, A. C. and Robertson, J. (2000) Interpretation of Raman spectra of disordered and amorphous carbon. Physical review B, 61, 14095.

Field, S. W. and Haggerty, S. E. (1990) Graphitic xenoliths from the Jagersfontein kimberlite, South Africa: evidence for dominantly anhydrous melting

and carbon deposition. Eos Transactions American Geophysical Union, 71, 658.

Frezzotti, M.-L., Huizenga, J.-M., Compagnoni, R., and Selverstone, J. (2014) Diamond formation by carbon saturation in C–O–H fluids during cold subduction of oceanic lithosphere. Geochimica et Cosmochimica Acta, 143, 68–86.

Glinnemann, J., Kusaka, K., and Harris, J. W. (2003) Oriented graphite single-crystal inclusions in diamond. Zeitschrift für Kristallographie/International journal for structural, physical, and chemical aspects of crystalline materials, 218, 733–739.

Golovin, A. V., Sharygin, V. V., and Pokhilenko, N. P. (2007) Melt inclusions in olivine phenocrysts in unaltered kimberlites from Udachnaya-East (Yakutia): some aspects of the evolution of kimberlite magmas in the late stages of crystallization. Petrologia, 15, 178–195.

Haggerty, S. E. (1986) Diamond genesis in a multiply-constrained model. Nature, pages 34–38.

Haggerty, S. E. (1999) A diamond trilogy: superplumes, supercontinents, and supernovae. Science, 285, 851–860.

Harris, J. W. (1972) Black material on mineral inclusions and in internal fracture planes in diamond. Contributions to Mineralogy and Petrology, 35, 22–33.

Harris, J. W. (1992) Diamond geology. The properties of natural and synthetic diamond, pages 345–393.

Harris, J. W. and Gurney, J. J. (1979) Inclusions in diamond. The properties of diamond, pages 555–591.

Harris, J. W. and Vance, E. R. (1972) Inclusions in diamond. Contribution Mineralogy Petrology, 115, 227–234.

Hatton, C. J. (1978) The geochemistry and origin of xenoliths from the Roberts Victor Mine. Ph.D. thesis, Geochemistry–University of Cape Town.

Hatton, C. J. and Gurney, J. J. (1979) A Diamond-Graphite Eclogite from the Roberts Victor Mine. The Mantle Sample: Inclusion in Kimberlites and Other Volcanics, pages 29–36.

Holland, T. J. B. (1980) The reaction albite= jadeite+ quartz determined experimentally in the range 600-1200 degrees C. American Mineralogist, 65, 129–134.

Holland, T. J. B. (1983) The experimental determination of activities in disordered and short-range ordered jadeitic pyroxenes. Contributions to Mineralogy and Petrology, 82, 214–220.

Jacob, D. E. and Foley, S. F. (1999) Evidence for Archean ocean crust with low high field strength element signature from diamondiferous eclogite xenoliths. Lithos, 48, 317–336.

Kamenetsky, V. S., Golovin, A. V., Maas, R., Giuliani, A., Kamenetsky, M. B., and Weiss, Y. (2014) Towards a new model for kimberlite petrogenesis: Evidence from unaltered kimberlites and mantle minerals. Earth-Science Reviews, 139, 145–167.

Kaminsky, F. V., Wirth, R., and Morales, L. (2013) Internal texture and syngenetic inclusions in carbonado. The Canadian Mineralogist, 51, 39–56.

Kennedy, C. S. and Kennedy, G. C. (1976) The equilibrium boundary between graphite and diamond. Journal of Geophysical Research, 81, 2467–2470.

Kharkiv, A. D., Zuenko, V. V., Zinchuk, N. N., Kryuchkov, A. I., Ukhanov, V. A., and Bogatykh, M. M. (1991) Petrochemistry of kimberlites. Nedra, Moscow, 304.

Khokhryakov, A. F. and Nechaev, D. V. (2015) Typomorphic features of graphite inclusions in diamond: experimental data. Russian Geology and Geophysics, 56, 232–238.

Khokhryakov, A. F., Nechaev, D. V., Sokol, A. G., and Pal'yanov, Y. N. (2009) Formation of various types of graphite inclusions in diamond: Experimental data. Lithos, 112, 683–689.

Khokhryakov, A. F., Pal'yanov, Y. N., and Sobolev, N. V. (2002) Crystal morphology as an indicator of redox conditions of natural diamond dissolution at the mantle PT parameters. Doklady earth sciences, 385, 534–537.

Kinny, P. D., Griffin, B. J., Heaman, L. M., Brakhfogel, F. F., and Spetsius, Z. V. (1997) SHRIMP U-Pb ages of perovskite from Yakutian kimberlites. Russian geology and geophysics, 38, 97–105.

Korsakov, A. V., Perraki, M., Zedgenizov, D. A., Bindi, L., Vandenabeele, P., Suzuki, A., and Kagi, H. (2010) Diamond–graphite relationships in ultrahigh-pressure metamorphic rocks from the Kokchetav Massif, Northern Kazakhstan. Journal of Petrology, 51, 763–783.

Korsakov, A. V., Zhimulev, E. I., Mikhailenko, D. S., Demin, S. P., and Kozmenko, O. A. (2015) Graphite pseudomorphs after diamonds: An experimental study of graphite morphology and the role of H2O in the graphitisation process. Lithos, 236, 16–26.

Kostrovitsky, S. I., Kopylova, M. G., Egorov, K. N., and Yakovlev, D. A. (2013) The exceptionally fresh Udachnaya-East kimberlite: evidence for brine and evaporite contamination. In Proceedings of 10th International Kimberlite Conference, pages 75–91. Springer.

Kostrovitsky, S. I., Morikiyo, T., Serov, I. V., Yakovlev, D. A., and Amirzhanov, A. A. (2007) Isotope-geochemical systematics of kimberlites and related rocks from the Siberian Platform. Russian Geology and Geophysics, 48, 272–290.

Kuharenko, A. A. (1955) Urals diamonds, volume 516. Moscow.

Lavrentev, Y. G., Karmanov, N., and Usova, L. (2015) Electron probe microanalysis of minerals: Microanalyzer or scanning electron microscope? Russian Geology and Geophysics, 56, 1154–1161.

Lespade, P., Al-Jishi, R., and Dresselhaus, M. S. (1982) Model for Raman scattering from incompletely graphitized carbons. Carbon, 20, 427–431.

Litvin, Y. A., Chudinovskikh, L. T., and Zharikov, V. A. (1997) Experimental Crystallization of Diamond and Graphite from Alkali-Carbonate Melts at 7-11 GPa. Russian Academii of Sciences, 355, 908–911.

Liu, Y., Taylor, L. A., Sarbadhikari, A. B., Valley, J. W., Ushikubo, T., Spicuzza, M. J., Kita, N., Ketcham, R. A., Carlson, W., Shatsky, V., et al. (2009) Metasomatic origin of diamonds in the world's largest diamondiferous eclogite. Lithos, 112, 1014–1024.

Logvinova, A. M., Wirth, R., Fedorova, E. N., and Sobolev, N. V. (2008) Nanometre-sized mineral and fluid inclusions in cloudy Siberian diamonds: new insights on diamond formation. European Journal of Mineralogy, 20, 317–331.

Luth, R. W. (1999) Carbon and carbonates in the mantle. Mantle Petrology: Field Observations and High Pressure Experimentation: A Tribute to Francis R.(Joe) Boyd, 6, 297–316.

Luth, R. W. (2001) Experimental determination of the reaction aragonite+ magnesite= dolomite at 5 to 9 GPa. Contributions to Mineralogy and Petrology, 141, 222–232.

Meyen, O. A. (1985) Genesis of diamond: a mantle saga. American Mineralogist, 70, 344–355.

Meyer, H. (1987) Inclusions in diamond. Mantle xenoliths, pages 501–522.

Naemura, K., Ikuta, D., Kagi, H., Odake, S., Ueda, T., Ohi, S., Kobayashi, T., Svojtka, M., and Hirajima, T. (2011) Diamond and other possible ultradeep evidence discovered in the orogenic spinel-garnet peridotite from the Moldanubian Zone of the Bohemian Massif, Czech Republic. Ultrahigh-Pressure Metamorphism, 25, 77–124.

Nasdala, L., Brenker, F. E., Glinnemann, J., Hofmeister, W., Gasparik, T., Harris, J. W., Stachel, T., and Reese, I. (2003) Spectroscopic 2D-tomography Residual pressure and strain around mineral inclusions in diamonds. European Journal of Mineralogy, 15, 931–935.

Nasdala, L., Hofmeister, W., Harris, J. W., and Glinnemann, J. (2005) Growth zoning and strain patterns inside diamond crystals as revealed by Raman maps. American Mineralogist, 90, 745–748.

Navon, O. (1999) Diamond formation in the Earth's mantle. In Proceedings of the 7th International Kimberlite Conference, volume 2, pages 584–604. Cape Town: Red Roof Design.

Nechaev, D. V. and Khokhryakov, A. F. (2013) Formation of epigenetic graphite inclusions in diamond crystals: experimental data. Russian Geology and Geophysics, 54, 399–405.

Nemanich, R. J. and Solin, S. A. (1979) First-and second-order Raman scattering from finite-size crystals of graphite. Physical Review B, 20, 392.

Nimis, P. and Taylor, W. R. (2000) Single clinopyroxene thermobarometry for garnet peridotites. Part I. Calibration and testing of a Cr-in-Cpx barometer and an enstatite-in-Cpx thermometer. Contributions to Mineralogy and Petrology, 139, 541–554.

Orlov, I. U. (1977) The mineralogy of the diamond. John Wiley & Sons.

Pal'yanov, N., Sokol, A. G., Borzdov, M., and Khokhryakov, A. F. (2002) Alkaline carbonate-fluid melts as the medium for the formation of diamonds in the Earths mantle: an experimental study . Lithos, 60, 145–159.

Pal'yanov, Y. N., Borzdov, Y. M., Khokhryakov, A. F., Kupriyanov, I. N., and Sobolev, N. V. (2006) Sulfide melts–graphite interaction at HPHT conditions: Implications for diamond genesis. Earth and Planetary Science Letters, 250, 269–280.

652 Pal'yanov, Y. N. and Sokol, A. G. (2009) The effect of composition of mantle
653 fluids/melts on diamond formation processes. Lithos, 112, 690–700.

654 Pal'yanov, Y. N., Sokol, A. G., Borzdov, Y. M., Khokhryakov, A. F., and
655 Sobolev, N. V. (1999) Diamond formation from mantle carbonate fluids. Na-
656 ture, 400, 417–418.

657 Pal'yanov, Y. N., Sokol, A. G., and Sobolev, N. V. (2005) Experimental model-
658 ing of mantle diamond-forming processes. Russian Geology and Geophysics,
659 46, 1271–1284.

660 Palyanov, Y. N., Sokol, A. G., Borzdov, Y. M., Khokhryakov, A. F., and
661 Sobolev, N. V. (2002) Diamond formation through carbonate-silicate interac-
662 tion. American Mineralogist, 87, 1009–1013.

663 Pasteris, J. D. and Wopenka, B. (2003) Necessary, but not sufficient: Raman
664 identification of disordered carbon as a signature of ancient life. Astrobiology,
665 3, 727–738.

666 Pearson, D. G., Boyd, F. R., Haggerty, S. E., Pasteris, J. D., Field, S. W.,
667 Nixon, P. H., and Pokhilenko, N. P. (1994) The characterisation and origin
668 of graphite in cratonic lithospheric mantle: a petrological carbon isotope and
669 Raman spectroscopic study. Contributions to Mineralogy and Petrology, 115,
670 449–466.

671 Pearson, D. G., Boyd, F. R., and Nixon, P. H. (1990) Graphite-bearing mantle
672 xenoliths from the Kaapvaal craton: implications for graphite and diamond
673 genesis. Annual Report of Director of the Geophysical Laboratory, 1990,
674 11–19.

675 Pearson, D. G., Kelley, S. P., Pokhilenko, N. P., and Boyd, F. R. (1997) Laser
676 40Ar/39Ar dating of phlogopites from Southern African and Siberian kim-
677 berlites and their xenoliths: constraints on eruption ages, melt degassing and
678 mantle volatile compositions. Russian Geology and Geophysics, 38, 106–117.

Pearson, D. G., Shirey, S. B., Bulanova, G. P., Carlson, R. W., and Milledge, H. J. (1999) Dating and paragenetic distinction of diamonds using the Re-Os isotope system; application to some Siberian diamonds. In Proceedings of the 7th International Kimberlite Conference, volume 2, pages 637–643.

Pokhilenko, N. P., Sobolev, N. V., Kuligin, S. S., and Shimizu, N. (1999) Peculiarities of distribution of pyroxenite paragenesis garnets in Yakutian kimberlites and some aspects of the evolution of the Siberian craton lithospheric mantle. In Proceedings of the 7th International Kimberlite Conference, volume 2, pages 689–698. Red Roof Design Cape Town.

Pokhilenko, N. P., Sobolev, N. V., and Yefimova, Y. S. (1982) Xenolith of deformed diamond-bearing kyanite eclogite from the Udachnaya pipe, Yakutia. In Doklady Akademii Nauk SSSR, volume 266, pages 212–216.

Pollack, H. N. and Chapman, D. S. (1977) On the regional variation of heat flow, geotherms, and lithospheric thickness. Tectonophysics, 38, 279–296.

Ravna, E. J. K. and Paquin, J. (2003) Thermobarometric methodologies applicable to eclogites and garnet ultrabasites. EMU notes in mineralogy, 5, 229–259.

Robinson, D., Gurney, J., and Shee, S. (1984) Diamond eclogite and graphite eclogite xenoliths from Orapa, Botswana, Kimberlites II: The Mantle and Crust-Mantle Relationships J. Kornprobst, 11–24.

Robinson, D. N. (1979) Diamond and graphite in eclogite xenoliths from kimberlite. The Mantle Sample: Inclusion in Kimberlites and Other Volcanics, pages 50–58.

Schrauder, M. and Navon, O. (1994) Hydrous and carbonatitic mantle fluids in fibrous diamonds from Jwaneng, Botswana. Geochimica et Cosmochimica Acta, 58, 761–771.

Sharma, S. K., Mao, H. K., Bell, P. M., and Xu, J. A. (1985) Measurement of stress in diamond anvils with micro-Raman spectroscopy. Journal of Raman spectroscopy, 16, 350–352.

Shatsky, V., Ragozin, A., Zedgenizov, D., and Mityukhin, S. (2008) Evidence for multistage evolution in a xenolith of diamond-bearing eclogite from the Udachnaya kimberlite pipe. Lithos, 105, 289–300.

Smyth, J. R. and Caporuscio, F. A. (1984) Petrology of a suite of eclogite inclusions from the Bobbejaan kimberlite: II. Primary phase compositions and origin. Kimberlites II: The mantle and crust-mantle relationships, pages 121–131.

Sobolev, A. V., Sobolev, N. V., Smith, C. B., and Dubessy, J. (1989) Fluid and melt compositions in lamproites and kimberlites based on the study of inclusions in olivine. In Proceedings of the 4th International Kimber lite Conference. Kimberlites and Related Rocks, pages 220–240.

Sobolev, N. V. (1974) Deep-seated inclusions in kimberlites and the problem of the Upper Mantle composition. 183. Nauka, 264 pages.

Sokol, A. G., Borzdov, Y. M., Pal'yanov, Y. N., Khokhryakov, A. F., and Sobolev, N. V. (2001a) An experimental demonstration of diamond formation in the dolomite-carbon and dolomite-fluid-carbon systems. European Journal of Mineralogy, 13, 893–900.

Sokol, A. G. and Pal'yanov, Y. N. (2004) Diamond crystallization in fluid and carbonate-fluid systems under mantle PT conditions: 2. An analytical review of experimental data. Geohimia, pages 1157–1172.

Sokol, A. G. and Pal'yanov, Y. N. (2008) Diamond formation in the system MgO–SiO_2–H_2O–C at 7.5 GPa and 1,600 ^{o}C. Contributions to Mineralogy and Petrology, 155, 33–43.

Sokol, A. G., Pal'yanov, Y. N., Pal'yanova, G. A., Khokhryakov, A. F., and Borzdov, Y. M. (2001b) Diamond and graphite crystallization from C–O–H

733 fluids under high pressure and high temperature conditions. Diamond and
734 Related Materials, 10, 2131–2136.

735 Sokol, A. G., Pal'yanov, Y. N., Pal'yanova, G. A., and Tomilenko, A. A. (2004)
736 Diamond crystallization in fluid and carbonate-fluid systems under mantle PT
737 conditions: 1. Fluid composition. Geochemistry International, 42, 830–838.

738 Spera, F. J. (1984) Carbon dioxide in petrogenesis III: role of volatiles in the
739 ascent of alkaline magma with special reference to xenolith-bearing mafic
740 lavas. Contributions to Mineralogy and Petrology, 88, 217–232.

741 Stagno, V., Frost, D., McCammon, C., Mohseni, H., and Fei, Y. (2015) The
742 oxygen fugacity at which graphite or diamond forms from carbonate-bearing
743 melts in eclogitic rocks. Contributions to Mineralogy and Petrology, 169,
744 1–18.

745 Stepanov, A. S., Korsakov, A. V., Yuryeva, O. P., Nadolinniy, V. A., Perraki,
746 M., De Gussem, K., and Vandenabeele, P. (2011) Brown diamonds from an
747 eclogite xenolith from Udachnaya kimberlite, Yakutia, Russia. Spectrochimica
748 Acta Part A: Molecular and Biomolecular Spectroscopy, 80, 41–48.

749 Stepanov, A. S., Shatsky, V. S., Zedgenizov, D. A., and Ragozin, A. L. (2008)
750 Chemical heterogeneity in the diamondiferous eclogite xenolith from the
751 Udachnaya kimberlite pipe. Doklady Earth Sciences, 419, 308–311.

752 Stepanov, A. S., Shatsky, V. S., Zedgenizov, D. A., and Sobolev, N. V. (2007)
753 Causes of variations in morphology and impurities of diamonds from the
754 Udachnaya Pipe eclogite. Russian Geology and Geophysics, 48, 758–769.

755 Sverjensky, D. A. and Huang, F. (2015) Diamond formation due to a pH drop
756 during fluid-rock interactions. Nature communications, 6.

757 Syracuse, E. M., van Keken, P. E., and Abers, G. A. (2010) The global range
758 of subduction zone thermal models. Physics of the Earth and Planetary
759 Interiors, 183, 73–90.

Taylor, L. A., Milledge, H. J., Bulanova, G. P., Snyder, G. A., and Keller, R. A. (1998) Metasomatic eclogitic diamond growth: evidence from multiple diamond inclusions. International Geology Review, 40, 663–676.

Taylor, L. A. and Neal, C. R. (1989) Eclogites with oceanic crustal and mantle signatures from the Bellsbank kimberlite, South Africa, Part I: mineralogy, petrography, and whole rock chemistry. The Journal of Geology, 97, 551–567.

Taylor, W. R., Jaques, A. L., and Ridd, M. (1990) Nitrogen-defect aggregation characteristics of some Australasian diamonds: time-temperature constraints on the source regions of pipe and alluvial diamonds. American Mineralogist, 75, 1290–1310.

Thomson, A. R., Walter, M. J., Kohn, S. C., and Brooker, R. A. (2016) Slab melting as a barrier to deep carbon subduction. Nature, 529, 76–79.

Titkov, S. V., Gorshkov, A. I., Solodova, Y. P., Ryabchikov, I. D., Magazina, L. O., Sivtsov, A. V., Gasanov, M. D., Sedova, E. A., and Samosorov, G. G. (2006) Mineral microinclusions in cubic diamonds from the Yakutian deposits based on analytical electron microscopy data. Doklady Earth of Sciences, 410, 1106–1108.

Tuinstra, F. and Koenig, J. L. (1970) Raman spectrum of graphite. The Journal of Chemical Physics, 53, 1126–1130.

Viljoen, K. S. (1995) Graphite-and diamond-bearing eclogite xenoliths from the Bellsbank kimberlites, Northern Cape, South Africa. Contributions to Mineralogy and Petrology, 121, 414–423.

Wang, Y., Alsmeyer, D. C., and McCreery, R. L. (1990) Raman spectroscopy of carbon materials: structural basis of observed spectra. Chemistry of Materials, 2, 557–563.

Wopenka, B. and Pasteris, J. D. (1993) Structural characterization of kerogens to granulite-facies graphite: applicability of Raman microprobe spectroscopy. The American Mineralogist, 78, 533–557.

Yamaoka, S., Kumar, M. D. S., Akaishi, M., and Kanda, H. (2000) Reaction between carbon and water under diamond-stable high pressure and high temperature conditions. Diamond and Related Materials, 9, 1480–1486.

Yamaoka, S., Kumar, M. D. S., Kanda, H., and Akaishi, M. (2002a) Crystallization of diamond from CO_2 fluid at high pressure and high temperature. Journal of crystal growth, 234, 5–8.

Yamaoka, S., Kumar, M. D. S., Kanda, H., and Akaishi, M. (2002b) Thermal decomposition of glucose and diamond formation under diamond-stable high pressure–high temperature conditions. Diamond and related materials, 11, 118–124.

Zedgenizov, D. A., Kagi, H., Shatsky, V. S., and Sobolev, N. V. (2004) Carbonatitic melts in cuboid diamonds from Udachnaya kimberlite pipe (Yakutia): evidence from vibrational spectroscopy. Mineralogical Magazine, 68, 61–73.

Zhang, Y. (1998) Mechanical and phase equilibria in inclusion–host systems. Earth and Planetary Science Letters, 157, 209–222.

List of Figures

This is a preprint, the final version is subject to change, of the American Mineralogist (MSA)
Cite as Authors (Year) Title. American Mineralogist, in press.
(DOI will not work until issue is live.) DOI: http://dx.doi.org/10.2138/am-2016-5657

880 # Figures

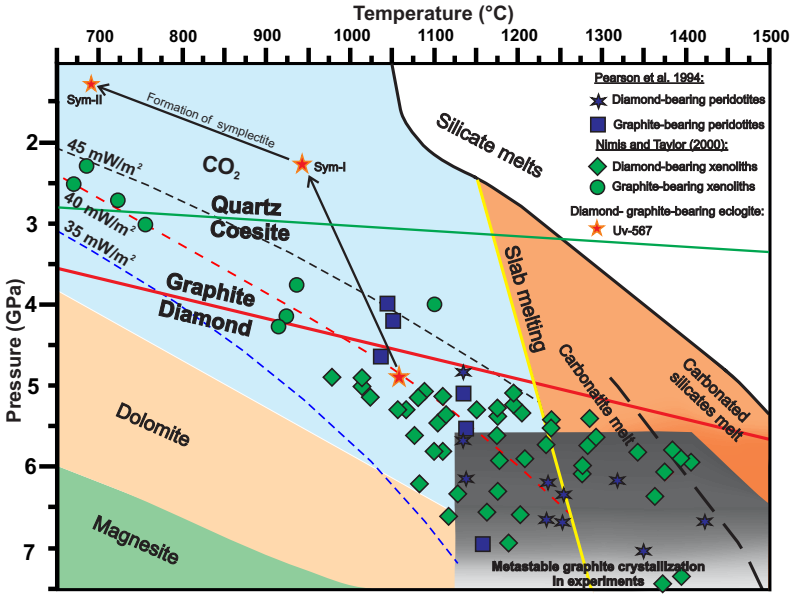

Figure 1: P-T conditions of formation for diamond- and graphite-bearing xenoliths from world-wide occurrence (Pearson et al., 1994; Nimis and Taylor, 2000) and the diamond- graphite-bearing eclogite sample Uv-567 of this study (red star). Symplectites I (SymI) and Symplectites II (SymII) are coarse- and fine-grained symplectites after omphacite, respectively. Metastable graphite crystallization field in experiments (Pal'yanov et al., 1999; Akaishi et al., 2000; Yamaoka et al., 2000; Akaishi and Yamaoka, 2000; Sokol et al., 2001a; Pal'yanov et al., 2002; Palyanov et al., 2002; Sokol and Pal'yanov, 2004)are shown as dark gray gradient areas. The stability fields of carbon-bearing phases are in different colors after Thomson et al. (2016). The melting curve of carbonated MORB compared to hot and cold subduction geotherms is according to (Syracuse et al., 2010). Quartz-coesite equilibrium is after Bose and Ganguly (1995); graphite-diamond equilibrium is after Kennedy and Kennedy (1976). Continental geotherm of 40 mW/m^2 heat flow is from Pollack and Chapman (1977).

This is a preprint, the final version is subject to change, of the American Mineralogist (MSA)
Cite as Authors (Year) Title. American Mineralogist, in press.
(DOI will not work until issue is live.) DOI: http://dx.doi.org/10.2138/am-2016-5657

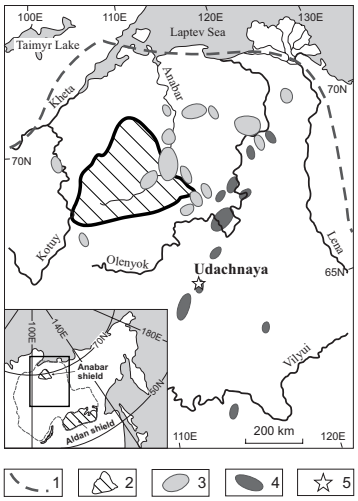

Figure 2: 1. Simplifed geology of the Siberian craton, showing craton boundaries (1), outcrops of Precambrian rocks (2), locations of Mesozoic (3) and Paleozoic (4) kimberlite fields, and the Udachnaya kimberlite pipe (5). Modifed after Pokhilenko et al. (1999).

Figure 3: A polished fragment of graphite- and diamond-bearing eclogitic xenolith (sample Uv-567) from Udachnaya-East kimberlite.

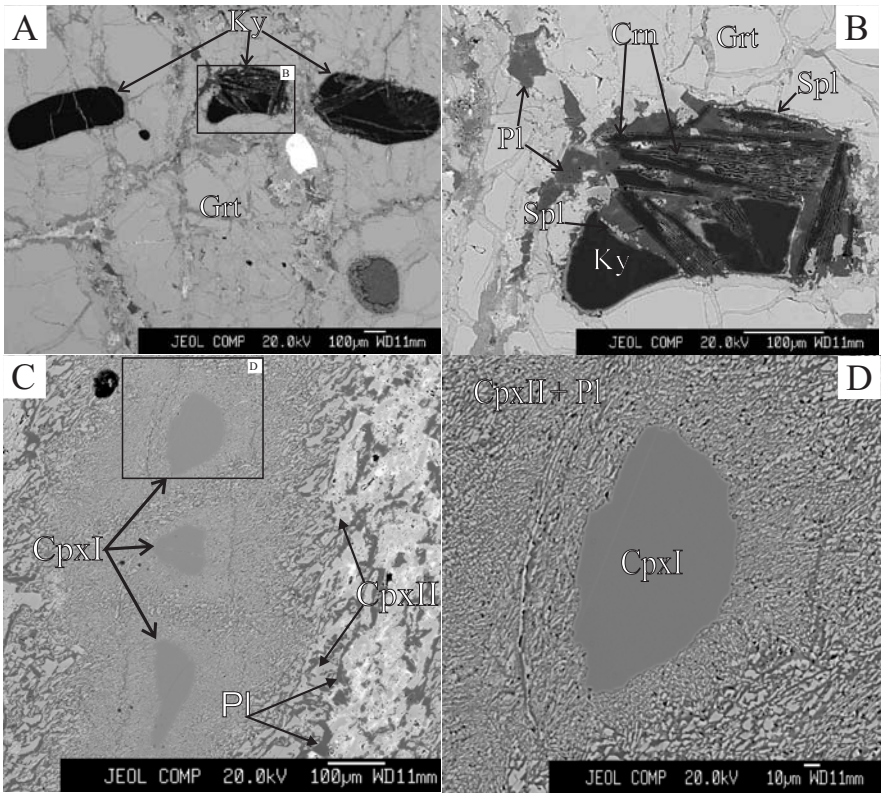

Figure 4: BSE images of plagioclase-spinel symplectite around primary kyanite inclusion in garnet (A-B) and fine diopside-plagioclase symplectite around residual omphacite (C-D) from Uv-567 eclogite. Note that secondary phases increase in size away from omphacite. Mineral abbreviations are Ky = kyanite; CpxI = omphacite; CpxII = diopside; Pl = plagioclase; Grt = garnet; Spl = spinel; Crn = corundum.

This is a preprint, the final version is subject to change, of the American Mineralogist (MSA)
Cite as Authors (Year) Title. American Mineralogist, in press.
(DOI will not work until issue is live.) DOI: http://dx.doi.org/10.2138/am-2016-5657

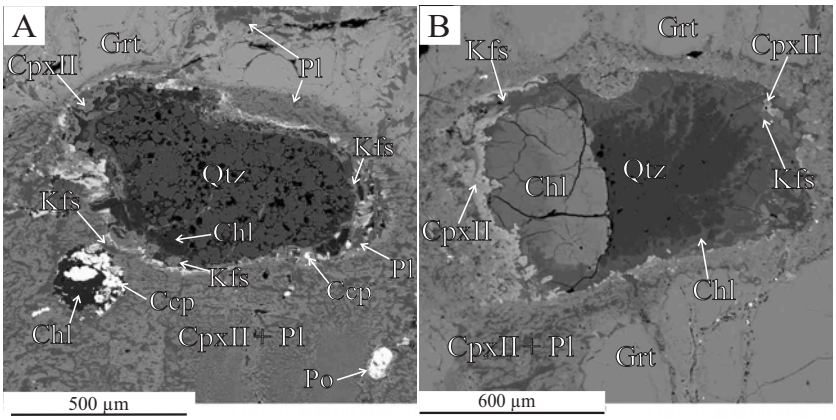

Figure 5: BSE images of secondary mineral assemblages around quartz (quartz pseudomorphs after coesite). A: coarse quartz grain at the boundary of garnet with diopside-plagioclase symplectite; B: quartz inclusion in garnet with typical alteration features. Mineral abbreviations are Qtz = quartz; p = chalcopyrite; Kfs = K-feldspar; Po = pentlandite; Chl = chlorite; CpxI = omphacite; CpxII = diopside; Pl = plagioclase; Grt = garnet; Spl = spinel; Rt = rutile; Bt = biotite; Cal = calcite; Ms = muscovite.

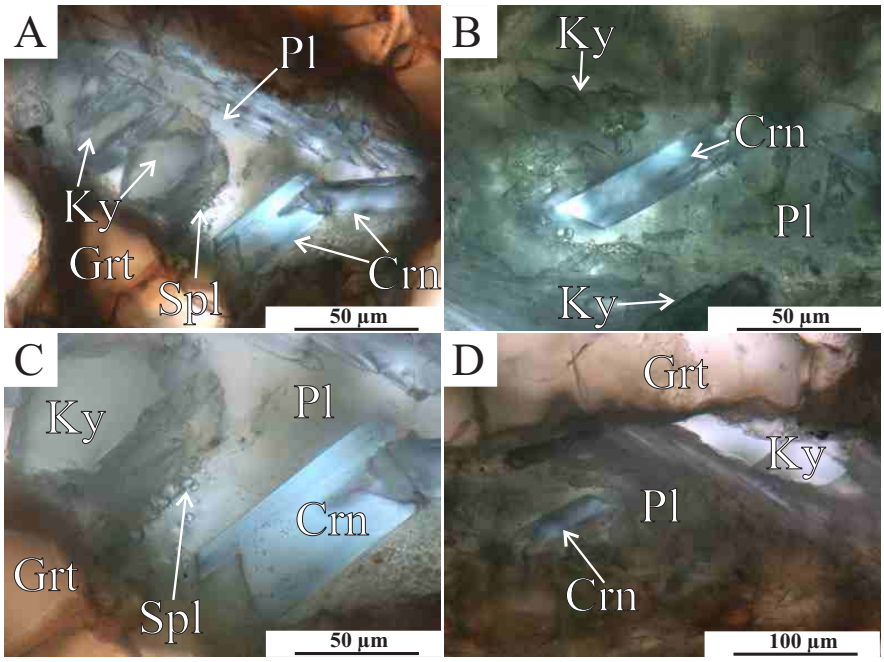

Figure 6: Photomicrographs of Plagioclase-spinel symplectite around residual kyanite (inclusion in garnet). Mineral abbreviations are Ky = kyanite; Pl = plagioclase; Grt = garnet; Spl = spinel; Crn = corundum.

This is a preprint, the final version is subject to change, of the American Mineralogist (MSA)
Cite as Authors (Year) Title. American Mineralogist, in press.
(DOI will not work until issue is live.) DOI: http://dx.doi.org/10.2138/am-2016-5657

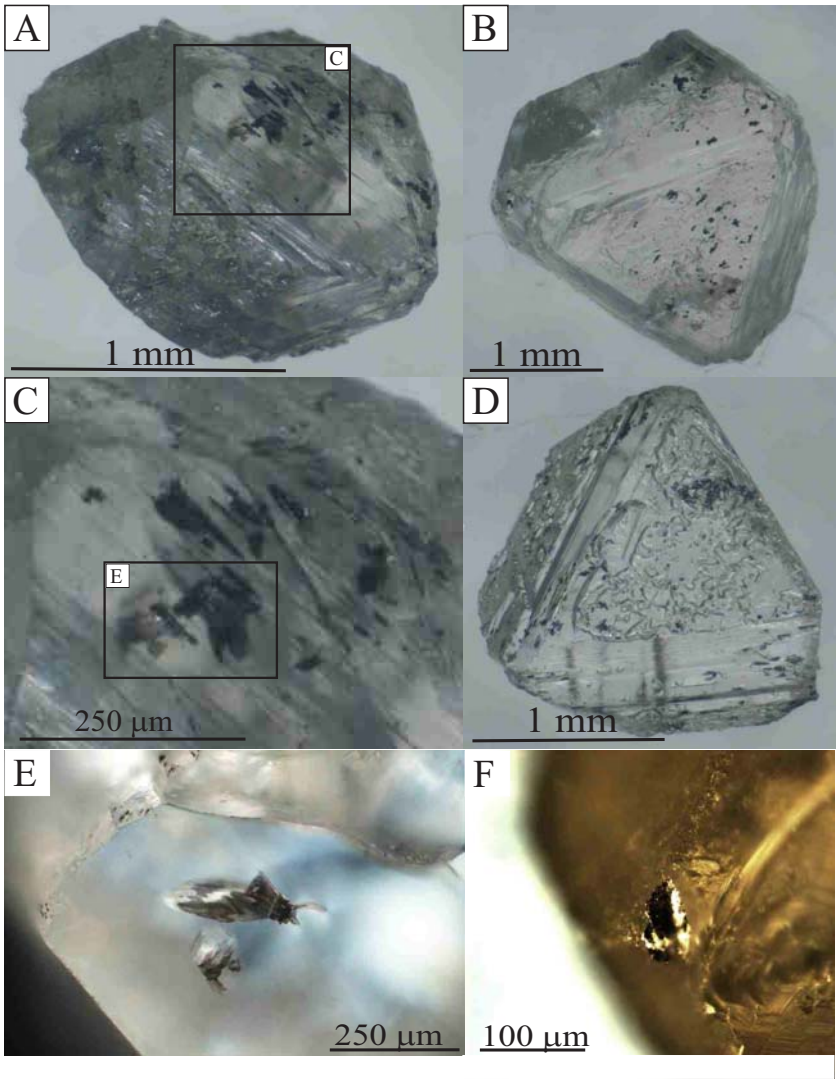

Figure 7: Photomicrographs of diamond crystals from sample Uv-567 (A, B, D); enlarged fragment with most abundant graphite inclusions (C); polished section of diamond crystal with large graphite inclusions (E); a graphite grain on a chip of a diamond crystal (F).

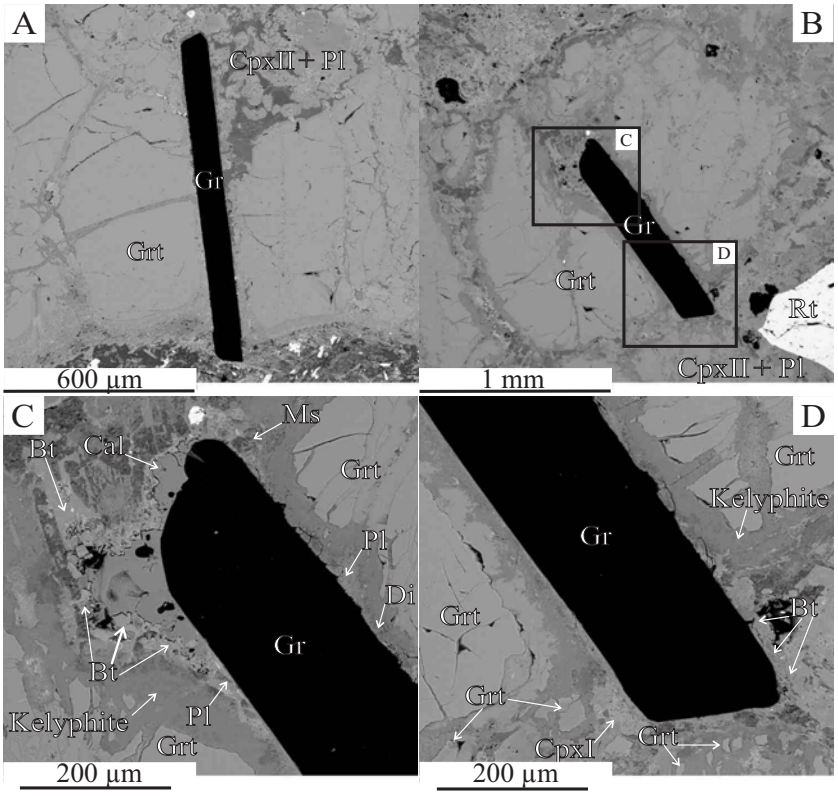

Figure 8: BSE images of a large euhedral graphite inclusion in garnet. Note that graphite is not fully buffered by garnet; there are secondary phases around primary graphite. Mineral abbreviations are Gr =graphite; CpxI = omphacite; CpxII = diopside; Pl = plagioclase; Grt = garnet; Spl = spinel; Rt = rutile; Bt = biotite; Cal = calcite; Ms = muscovite.

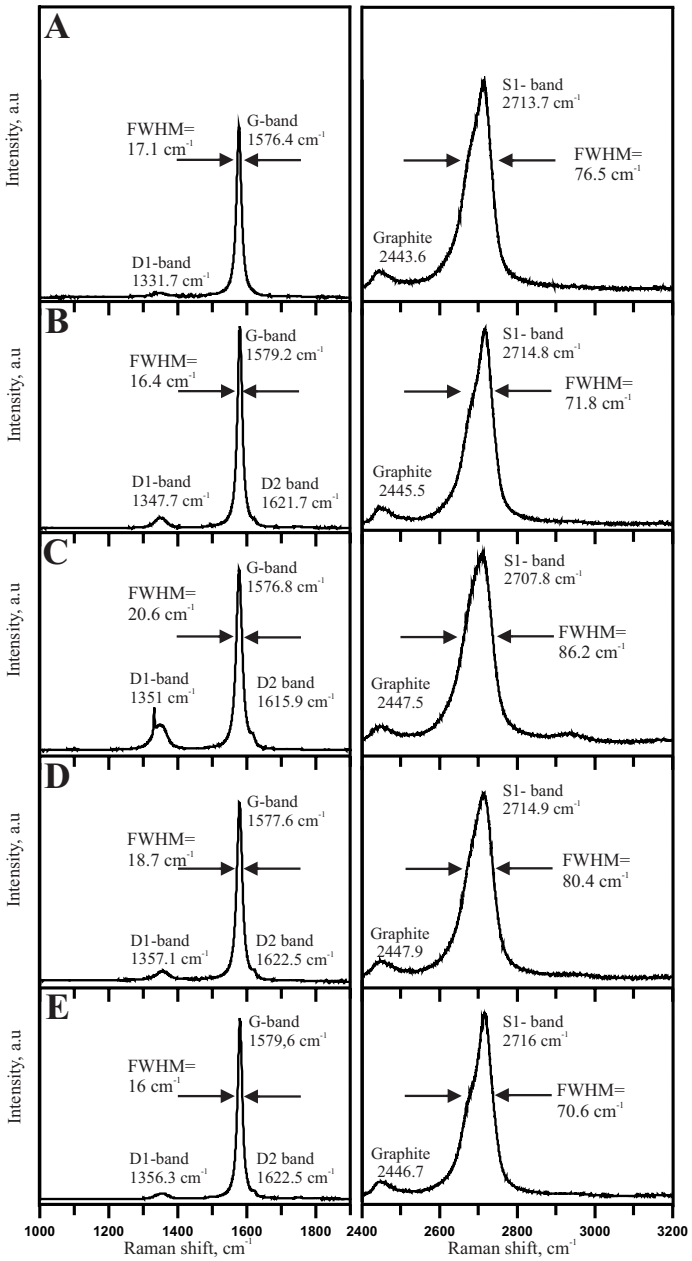

Figure 9: Representative Raman spectra of graphite crystals identified in eclogite xenolith Uv-567. A: graphite enclosed in diamond; B-E: graphite on diamond surfaces.

This is a preprint, the final version is subject to change, of the American Mineralogist (MSA)
Cite as Authors (Year) Title. American Mineralogist, in press.
(DOI will not work until issue is live.) DOI: http://dx.doi.org/10.2138/am-2016-5657

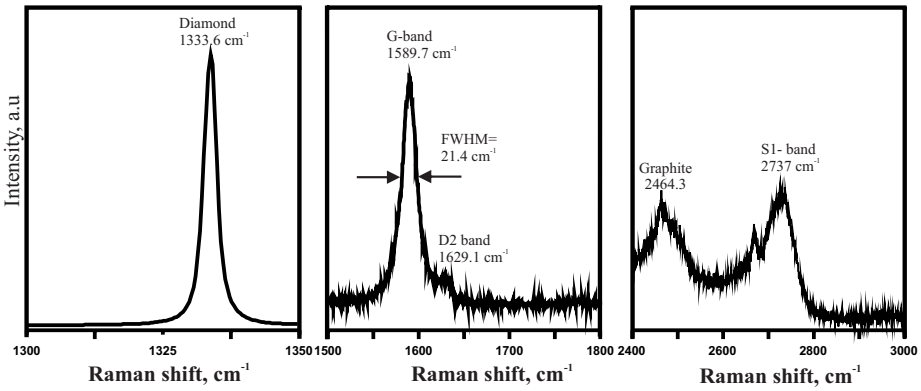

Figure 10: Raman spectra of graphite inclusion in diamond.

This is a preprint, the final version is subject to change, of the American Mineralogist (MSA)
Cite as Authors (Year) Title. American Mineralogist, in press.
(DOI will not work until issue is live.) DOI: http://dx.doi.org/10.2138/am-2016-5657

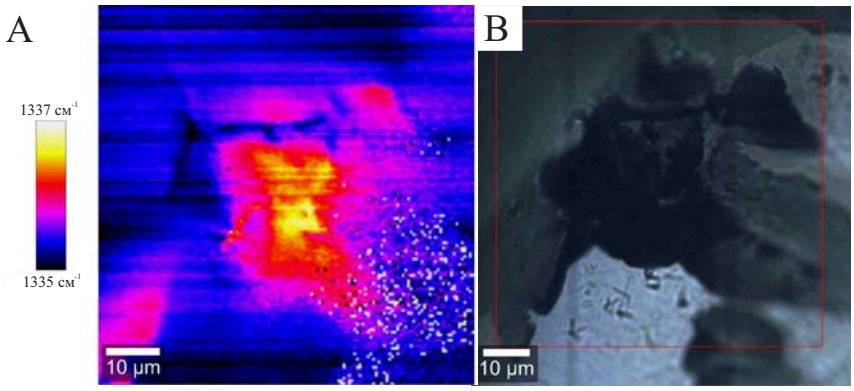

Figure 11: Raman map of a diamond crystal with graphite inclusions with the same area as shown in Figure A, based on the frequency of the LO=TO phonon. Areas without notable strain are visualized dark-blue (measured Raman shift 1335 cm^{-1}). Micro-areas affected by compressive strain (i.e., remnant internal pressure) are pink-yellow, and those affected by strong dilative strain (close to the ends of fractures) are red-yellow.

This is a preprint, the final version is subject to change, of the American Mineralogist (MSA)
Cite as Authors (Year) Title. American Mineralogist, in press.
(DOI will not work until issue is live.) DOI: http://dx.doi.org/10.2138/am-2016-5657

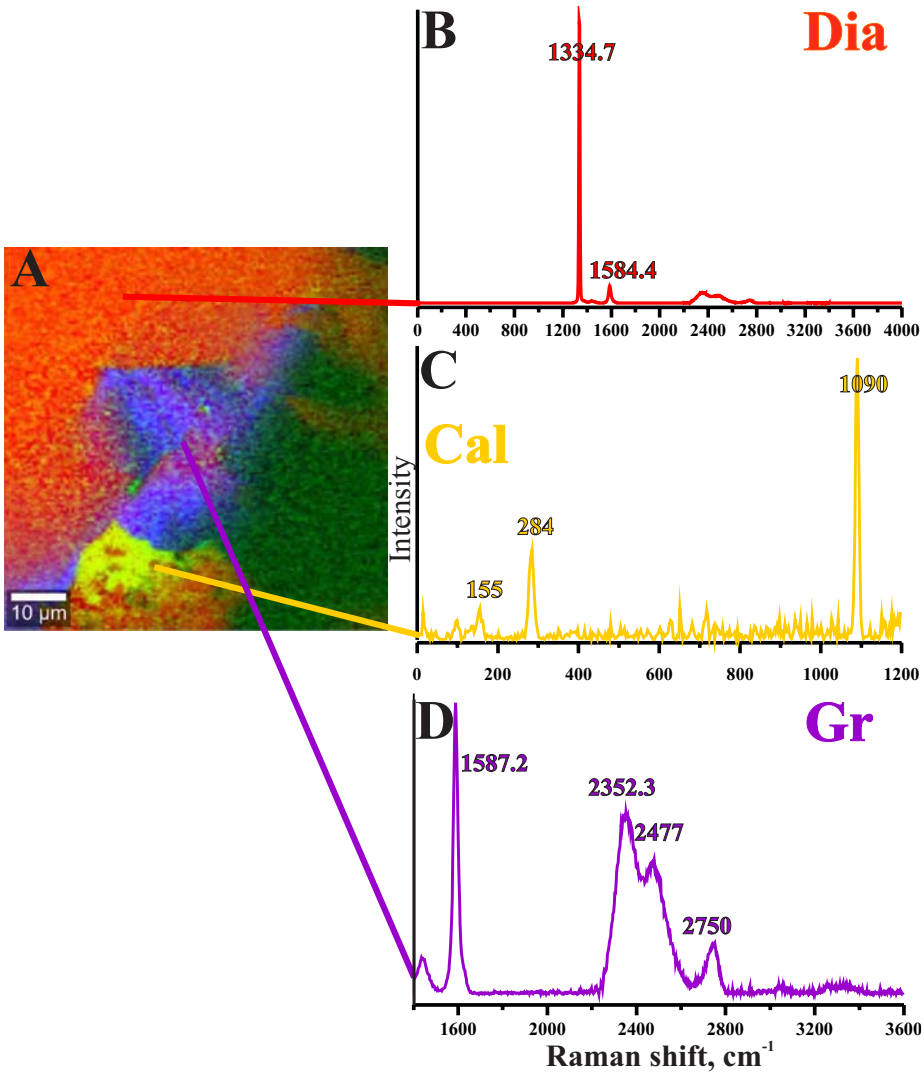

Figure 12: Raman image and individual Raman spectra inclusions of diamond, calcite and graphite. A: Raman map of diamond crystal with a graphite inclusion and a calcite inclusion next to it; B: Raman spectra of a diamond around graphite and calcite inclusions; C: Raman spectra of calcite inclusion in the range 0 to 1200 $^{-1}$; D: Raman spectra of graphite and calcite inclusion in the range 1500 cm^{-1} to 3600 $^{-1}$.

This is a preprint, the final version is subject to change, of the American Mineralogist (MSA)
Cite as Authors (Year) Title. American Mineralogist, in press.
(DOI will not work until issue is live.) DOI: http://dx.doi.org/10.2138/am-2016-5657

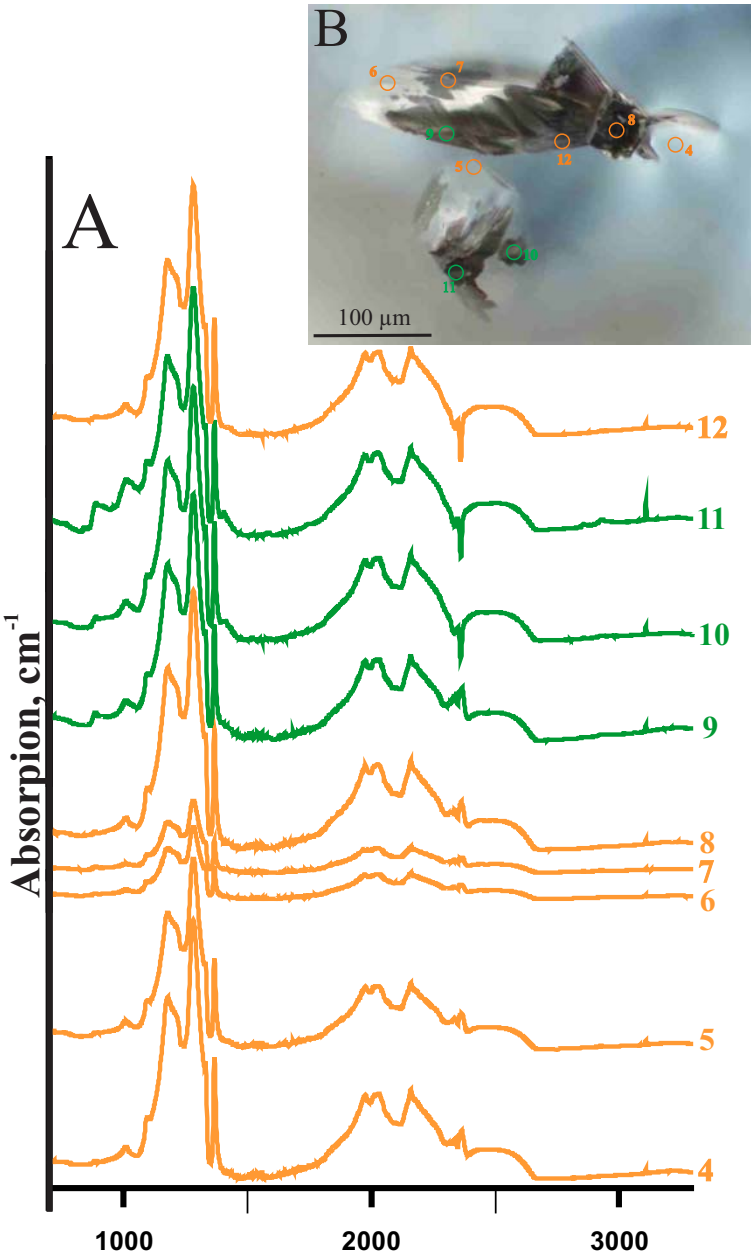

Figure 13: A: FTIR spectra of diamond with most abundant graphite inclusions in eclogite sample UV-567; B: FTIR data points in a diamond crystal that encloses graphite (with FTIR spectra points). Green circles mark points with peaks at 900-1000 cm^{-1}.

This is a preprint, the final version is subject to change, of the American Mineralogist (MSA)
Cite as Authors (Year) Title. American Mineralogist, in press.
(DOI will not work until issue is live.) DOI: http://dx.doi.org/10.2138/am-2016-5657

Table 1. Mineral major-element (wt.%) compositions of Uv-567

	SiO2	TiO2	Al2O3	Cr2O3	FeO	MnO	MgO	CaO	Na2O	K2O	Nb2O5	BaO	Cl	Total
Grt-R	40.5	0.2	22.3	0.06	12.5	0.2	11.3	13.0	0.1	0.01	--	--	--	100.2
Grt-C	40.8	0.2	22.6	0.07	12.5	0.2	11.5	12.9	0.1	0.00	--	--	--	100.9
Grt-R	40.0	0.2	22.8	0.07	12.3	0.2	10.6	12.9	0.2	0.03	--	--	--	99.3
Cpx-R	56.3	0.2	14.2	0.02	1.7	0.02	7.4	11.8	7.8	0.07	--	--	--	99.5
Cpx-C	56.3	0.2	14.1	0.04	1.8	0.02	7.3	11.7	7.8	0.08	--	--	--	99.3
Cpx-R	56.3	0.2	14.1	0.05	1.7	0.03	7.4	11.7	7.7	0.1	--	--	--	99.2
Pl	66.1	0.3	15.4	0	1.4	0.2	1.0	0.5	0.1	14.4	--	--	--	99.4
Pl	66.4	0.05	20.1	0.00	0.1	0.01	0.01	1.2	10.8	0.7	--	--	--	99.4
Spl	3.2	0.03	63.9	0.12	19.0	0.2	14.3	0.1	0.0	0.4	--	--	--	101.2
Crn	0.2	0.3	97.1	0.23	0.4	0.00	0.15	0.00	0	0	--	--	--	98.4
Crn	0	0.00	97.4	0.15	0.33	0.02	0.01	0.03	0	0	--	--	--	97.9
Ms	32.2	0.00	25.1	0.00	4.6	0.00	21.9	0	0.2	8.1	0.5	6.3	0	99.0
Bt	40.4	0.3	23.4	0.00	11.4	0.3	8.9	6.0	0.3	6.1	0	0	0.2	97.3
Kfsp	63.9	0.00	15.6	0.00	1.8	0.00	6.6	0	0.2	13.0	--	--	--	101.1
Rt-C	100	0.00	0	0.44	0	0.00	0	0	0	--	--	--	--	100.4

Note: C, core; R, rims; Grt, garnet; Cpx, clinopyroxene; Pl, plagioclase; Spl, spinel; Crn, corundum; Ms, muscovite; Bt, biotite;Kfsp, potassium feldspar; Rt, rutile.